2023 7th International Symposium on Innovative Approaches in Smart Technologies (ISAS) | 979-8-3503-8306-5/23/$31.00 ©2023 IEEE | DOI: 10.1109/ISAS60782.2023.10391097

Enhancing Trajectory Following in VTOL Cargo UAVs: Adaptive Control in Changing Payload Scenarios

1st Ahmet Sadık DURU
Mechanical Engineering Department
Ankara Yıldırım Beyazıt University
Ankara, Turkey
https://orcid.org/ 0000-0001-9142-9344

2nd Tolga ÖZASLAN
Mechanical Engineering Department
Ankara Yıldırım Beyazıt University
Ankara, Turkey
https://orcid.org/0000-0002-5002-0670

3rd Servet SOYGÜDER
Industrial Engineering Department
Ankara Yıldırım Beyazıt University
Ankara, Turkey
https://orcid.org/ 0000-0002-8191-6891

***Abstract*—This paper addresses the issue of controller performance degradation in cargo unmanned aerial vehicles (UAVs) due to varying payload amounts during a continuous flight. Linear controllers, such as PID, are often favored for non-aggressive UAV flights due to their simplicity and satisfactory performance compared to more complex alternatives. However, Vertical Takeoff and Landing (VTOL) cargo UAVs, while in operation, need to accommodate payloads of different masses, altering the flight dynamics. To maintain trajectories with an acceptable error margin, controller parameters, otherwise assumed constant, must be updated. In this study, we employ the meta-heuristic Gray Wolf Optimization technique to precompute PID parameter sets for a range of payloads in a 36-dimensional space, storing them in a look-up table (LUT). As the payload changes, we update cascade PID controller gains by interpolating LUT values. The proposed technique's performance is demonstrated through simulations involving various trajectories and payloads.**

***Index Terms*—Unmanned Aerial Vehicle, Cargo Quadcopter, Meta-heuristic Optimization, Gray Wolf Optimization, Cascade Controller**

I. Introduction

In recent years, there has been a growing interest in Vertical Takeoff and Landing (VTOL) Unmanned Aerial Vehicles (UAVs) owing to their manufacturability, agility, autonomous flight capabilities, and diverse payload carrying options [1]–[3]. UAVs present an alternative mode for transporting payloads over short to moderate distances, complementing traditional land and sea vehicles. For instance, the transportation of time-critical emergency supplies to search and rescue operations in a crisis area using UAVs may emerge as the sole alternative. This is particularly relevant when highways and railways are partially or completely demolished, rendering traditional transportation modes ineffective. Hence UAVs offer a valuable alternative for cargo transportation in regions where other means of transportation face hindrances, whether partial or complete.

Cargo UAVs operating continuously face the challenge of accommodating payloads with varying geometries and masses, consequently influencing the overall linear and rotational inertia of the entire system, along with changes in drag coefficients. The type of connection between a UAV and its payload, whether non-rigid or rigid, further impacts the system dynamics. For instance, a payload connected via a string introduces oscillating relative motion, disturbing UAV motion with fluctuating forces. In contrast, a rigidly connected payload directly alters the mass and rotational inertia, often treated not as a disturbance but as an additional mass. The dynamic coupling nature between the UAV and payload necessitates adaptive control strategies for the controller to effectively follow a given trajectory with limited error margins.

Linear controllers, like PID, are commonly chosen for UAV flights due to their simplicity and effectiveness. The extensive literature available on this specific application and in various robotic domains, along with their independence from underlying system complexities, contributes to their popularity. However, for a non-trivial system like a 6 degrees-of-freedom (DoF) UAV, the number of parameters becomes impractical for manual tuning. This challenge is especially prominent in UAVs employing a cascaded control scheme for attitude and position controls, where the parameter space expands to 36 dimensions as in our case.

In this study, we investigate a scenario in which a cargo UAV navigates through various trajectories while experiencing changing mass conditions during the flight. The onboard PID controller, upon detecting a change in the overall system mass, dynamically updates its parameters by referencing a precomputed look-up table (LUT) of parameters optimized offline using a meta-heuristic gray wolf optimization approach for different additional masses attributed to payload variations. In instances where a perfect fit is not feasible, we employ linear interpolation between the nearest points in the LUT. Simulation results reveal that PID parameters optimized for unloaded flight result in substantial offsets between desired and actual trajectories. Through the implementation of adaptive PID gains, the errors are contained within an acceptable envelope, ensuring safe and accurate flights.

The contributions of this paper are twofold: (1) we introduce

a novel controller design that dynamically adapts to changes in the mass and rotational inertia of a UAV in real-time during operation, (2) we utilize the GWO technique to precompute a large set of cascade PID control gains for various mass and rotational inertia values and store them in a fast LUT, enabling quick updates without the need for slow optimization steps during payload transportation.

II. Literature Review

Payload transportation using autonomous UAVs requires careful design of onboard controllers adaptive to disturbances induced by the relative motion of non-rigidly connected payloads, or changes in the overall mass and rotational inertia due of the system to rigidly connected cargo [4]. Ensuring the safety of both the UAV and the cargo is contingent on the system's ability to follow commanded trajectories with acceptable error margins.

Several studies in the literature realize payload transportation using multi-rotor UAVs [5]–[7] while majority of the related literature focuses carrying payloads rigidly attached to the a UAV [8]. In an alternative approach payloads are connected to the UAV through string allowing the payload to oscillate during flight reducing the coupling between the UAV and payload dynamics [9]. Cable suspended payloads cause oscillating disturbance on the UAVs and different approaches such [10]–[12] study this in details. Payload transportation with the help of extra mechanisms such as robot manipulators [13], [14] gripers [15], and magnetic grippers [16] are also studied by researchers.

In the work Son et. al. [17], the transport of a payload connected to a multi-rotor with a cable where a sequential linear quadratic solver along with the model predictive controller was used to calculate the optimal trajectory in real-time. In the work of Xie et al. [18] two different drones were used to carry the payload connected to a rope and formation control based on the leader follower approach. However, it is acknowledged that controlling multi-robot systems is challenging, primarily due to the additional complexity introduced by the coordination of multiple platforms.

Li et al. [19] employed the perception-constrained model predictive control (PCMPC) method as their controller. According to this method, the payload attached to the quadcopter operates in a manner that ensures it remains within the camera's field of view horizontally, ensuring continuous visibility. In a similar study Tang et al. [20] showed that they controlled the payload attached to the quadrotor with a cable under aggressive flight conditions. The control of the system is provided with a closed-loop geometric controller. Miyazaki et al. [15] in their study, while the multi-rotor is in motion, controlling the oscillation of the gripper can pick the payload at a point and take it to the target point and place it. Swing-suppression control method was implemented in the study . In these systems, the mass of the system remains constant while external disturbances oscillate due to the swinging motion of the payload. Unlike our work, these studies primarily focus on systems with constant mass and rotational inertia, concentrating solely on the control of a UAV under oscillating loads.

Liang et al. [21] designed an enhanced coupling hierarchical control system based on energy minimization to control the position of a single quadcopter and dampen the oscillation of a swinging payload connected to the quadcopter with a cable. In a similar study [22], control of a quadcopter carrying a suspended load and the absorption of the swing were achieved using the exponential regulation control method. Due to the coupled and underactuated dynamic structure of the system, designing this controller posed challenges, leading to the division of the controller into two parts: the inner loop and the outer loop. The inner loop controls the attitude of the UAV, while the outer loop controls the position of the UAV and the swing of the payload, which aligns with the strategy adopted in our work.

Slabber and Jordan [23] conducted simulation studies to investigate the control of a multirotor while a payload attached to a cable affects the dynamics of the multirotor during movement, especially when the length of the cable and the mass of the suspended payload are unknown. They employed the linear quadratic Gaussian (LQG) method along with a notch filter to mitigate the effects caused by the vibration and swinging motion of the load. The mass of the load was determined using the recursive least square method, and the length of the string was determined by a specialized sine wave estimator. State estimation of the load was achieved using vision-based optimal control (LQG) based on the obtained parameters of the payload. Our work differs from [23] in the availability of the mass information for the attached payload.

Similar to our approach, Wehbeh et al. [24] rigidly connected the payload to the drones using rigid bars and applied model predictive control (MPC). A comparison was made between centralized and decentralized MPC using a system consisting of four drones. Unlike our assumption on availability of force sensors for detecting the payload mass, Sanalitro et al. [25] employed control algorithms to ensure system control without using force or torque sensors. The cascade control method was utilized to apply a control algorithm based on the unexpected collision interaction scenario.

III. Mathematical Model of Quadcopter

A. Quadcopter Description

As can be seen "Fig. 1", quadcopter with X configuration structure has four rotors to generate the necessary thrust forces and torques. It produces thrust forces that are along the basis vector $-z^{\mathcal{B}}$ where the forces are denotes as F_1, F_2, F_3, and F_4. The forces consist of two pairs, F_1, F_3 and F_2, F_4. If one pair rotates clockwise the other rotates counterclockwise so the torques are balanced. Rolling, pitching, yawing motions can be realized by adjusting the speed of appropriate pairs of propellers.

The origins of the inertial and the body fixed frames are represented by $o^{\mathcal{I}}$ and $o^{\mathcal{B}}$ respectively.

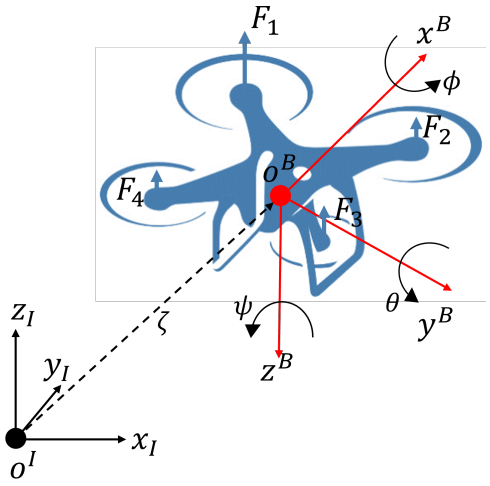

Fig. 1. Definition of inertial and body-fixed frame axes for an x-configuration quadcopter.

B. Quadcopter Kinematic Model

The structure of a quadcopter is shown in "Fig. 1". To describe the dynamics of a quadcopter, we need to define two reference frames which are the body and the inertial frames. Physical properties of a quadcopter are measured with respect to inertial frame or body frame depending on the formulation. Position and linear velocity are transformed across different frames by using a rotation matrix. Rotation matrix is constructed through application of three consecutive rotations about z, y, and x axes respectively as given below

$$\mathbf{R}_{\mathcal{B}}^{\mathcal{I}} = \begin{bmatrix} c\theta c\psi & c\psi s\theta s\phi - c\phi s\psi & c\phi c\psi s\theta + s\phi s\psi \\ c\theta s\psi & c\phi c\psi + s\theta s\phi s\psi & -c\psi s\phi + c\phi s\theta s\psi \\ -s\theta & c\theta s\phi & c\theta c\phi \end{bmatrix} \quad (1)$$

where c, s are trigonometric functions cosine, sine respectively. $\mathbf{R}_{\mathcal{B}}^{\mathcal{I}}$ represents a rotation transformation from body to inertial frame, roll (ϕ), pitch (θ), and yaw (ψ) denote Euler angles. Roll ϕ, pitch θ, and yaw ψ represent angle of rotation around x, y and z axes respectively.

The position $\boldsymbol{\zeta}$, linear velocity $\boldsymbol{V}$, attitude $\boldsymbol{\eta}$, angular velocity $\boldsymbol{\omega}$ are all three-vectors and defined as

$$\boldsymbol{\zeta}^{\mathcal{I}} = \begin{bmatrix} x \\ y \\ z \end{bmatrix}, \boldsymbol{V}^{\mathcal{B}} = \begin{bmatrix} u \\ v \\ w \end{bmatrix}, \boldsymbol{\eta}^{\mathcal{I}} = \begin{bmatrix} \phi \\ \theta \\ \psi \end{bmatrix}, \boldsymbol{\omega}^{\mathcal{B}} = \begin{bmatrix} p \\ q \\ r \end{bmatrix}.$$

The superscripts represent the frame with respect to which each vector is defined. In the following sections we drop superscripts unless required. The angular velocity is transformed from the inertial frame to the body frame by the transformation matrix $\mathbf{T}$ as follows

$$\dot{\boldsymbol{\eta}} = \mathbf{T}\boldsymbol{\omega}, \begin{bmatrix} \dot{\phi} \\ \dot{\theta} \\ \dot{\psi} \end{bmatrix} = \begin{bmatrix} 1 & s\phi t\theta & c\phi t\theta \\ 0 & c\phi & -s\phi \\ 0 & s\phi/c\theta & c\phi/c\theta \end{bmatrix} \begin{bmatrix} p \\ q \\ r \end{bmatrix} \quad (2)$$

$$\boldsymbol{\omega} = \boldsymbol{T}^{-1}\dot{\boldsymbol{\eta}}, \begin{bmatrix} p \\ q \\ r \end{bmatrix} = \begin{bmatrix} 1 & 0 & -s\theta \\ 0 & c\phi & c\theta s\phi \\ 0 & -s\phi & c\theta c\phi \end{bmatrix} \begin{bmatrix} \dot{\phi} \\ \dot{\theta} \\ \dot{\psi} \end{bmatrix} \quad (3)$$

where t is the tangent function. The matrix $\mathbf{T}$ is invertible if $\theta \neq (2k-1)\frac{\pi}{2}$ where $k \in \mathbf{Z}$. A similar relation can be written for $\dot{\boldsymbol{\zeta}}^{\mathcal{I}}$ and $\boldsymbol{V}^{\mathcal{B}}$ as

$$\dot{\boldsymbol{\zeta}}^{\mathcal{I}} = \mathbf{R}_{\mathcal{B}}^{\mathcal{I}} V^{\mathcal{B}}. \quad (4)$$

Finally first-order terms in $\mathcal{I}$ are obtained in terms of respective terms defined in $\mathcal{B}$ as

$$\begin{aligned} \dot{x} &= [c\theta c\psi]u + [c\psi s\theta s\phi - c\phi s\psi]v \\ &\quad + [c\phi c\psi s\theta + s\phi s\psi]w \\ \dot{y} &= [c\theta s\psi]u + [c\phi c\psi + s\theta s\phi s\psi]v \\ &\quad + [c\phi s\theta s\psi - c\psi s\phi]w \\ \dot{z} &= [-s\theta]u + [c\theta s\phi]v + [c\theta c\phi]w \\ \dot{\phi} &= p + [s\phi t\theta]q + [c\phi t\theta]r \\ \dot{\theta} &= [c\phi]q - [s\phi]r \\ \dot{\psi} &= [sc\theta s\phi]q + [sc\theta c\phi]r \end{aligned} \quad (5)$$

C. Quadcopter Dynamic Model

Newton-Euler approach is used in order to obtain the dynamic model of quadcopter in (6) and (7). In addition, the dynamic model of quadcopter is obtained and verified by Euler-Lagrange method. A number of assumptions have been made to simplify the non-linear dynamic model

- quadcopter body structure is assumed to be rigid,
- quadcopter frame and its mass distribution is symmetrical about its center of gravity,
- body frame and quadcopter's center of mass are coincident,
- rotors of the quadcopter are equivalent,
- the rotors are parallel to $z^{\mathcal{B}}$,
- gyroscopic effects of all rotors and ground effect have been neglected.

Translational equation of motion of a quadcopter is given as

$$m\ddot{\boldsymbol{\zeta}} = mg \begin{bmatrix} 0 \\ 0 \\ 1 \end{bmatrix}^{\mathcal{I}} - \mathbf{R}_{\mathcal{B}}^{\mathcal{I}}\mathbf{U}_1 + \mathbf{R}_{\mathcal{B}}^{\mathcal{I}}\mathbf{F}_{\omega} \quad (6)$$

where g and $\mathbf{U}_1^{\top} = \begin{bmatrix} 0 & 0 & F_T \end{bmatrix}$ are gravitational acceleration and the total thrust vector generated by the rotors respectively, $F_T = F_1 + F_2 + F_3 + F_4$ is the magnitude of the total thrust produced by the rotors, $\mathbf{F}_{\omega}^{\top} = \begin{bmatrix} F_{\omega x} & F_{\omega y} & F_{\omega z} \end{bmatrix}$ are disturbance forces due to wind and other external factors. Euler's equation governing the rotational dynamics expressed in $\mathcal{B}$ is given as

$$\mathbf{U}_T - \boldsymbol{\tau}_g + \boldsymbol{\tau}_{\omega} = \mathbf{I}\dot{\boldsymbol{\omega}} + \boldsymbol{\omega} \times (\mathbf{I}\boldsymbol{\omega}) \quad (7)$$

where $\mathbf{U}_T^{\top} = \begin{bmatrix} U_2 & U_3 & U_4 \end{bmatrix}$ is the moments generated by the propellers, $\mathbf{I}$ is the inertial tensor, $\boldsymbol{\tau}_g$ and $\boldsymbol{\tau}_{\omega}$ are moment vectors for gyroscopic effects due to motors and moments due to wind affecting on the quadcopter respectively.

Expanding the equations 6-7 we obtain the following second-order differential equations for each DoF of the quadcopter as

$$\begin{aligned}
\ddot{x} &= \frac{-F_T}{m}[s\phi s\psi + c\phi c\psi s\theta] \\
\ddot{y} &= \frac{F_T}{m}[s\phi c\psi - c\phi s\psi s\theta] \\
\ddot{z} &= g - \frac{F_T}{m}[c\phi c\theta] \\
\ddot{\phi} &= \frac{U_2}{I_x} + \frac{I_y - I_z}{I_x}\dot{\theta}\dot{\psi} \\
\ddot{\theta} &= \frac{U_3}{I_y} + \frac{I_z - I_x}{I_y}\dot{\phi}\dot{\psi} \\
\ddot{\psi} &= \frac{U_4}{I_z} + \frac{I_x - I_y}{I_z}\dot{\phi}\dot{\theta}
\end{aligned} \quad . \tag{8}$$

We assume that external disturbances are negligible; therefore, they do not appear in the above equations. At hover state, we assume $\phi \approx 0$, $\theta \approx 0$ which yield the following approximations

$$\begin{aligned}
\begin{bmatrix}\dot{\phi} & \dot{\theta} & \dot{\psi}\end{bmatrix}^\top &\approx \begin{bmatrix}p & q & r\end{bmatrix}^\top \\
\begin{bmatrix}\dot{x} & \dot{y} & \dot{z}\end{bmatrix}^\top &\approx \begin{bmatrix}u & v & w\end{bmatrix}^\top
\end{aligned}$$

D. Linear Time Varying State-Space Model

The state space representation allows for expressing an n^{th} order system with n first-order differential equations which simplifies analysis of the respective system. Additionally, this approach effectively captures input-output relations of multiple-input-multiple-output system as in our case. Furthermore, modeling time-varying mechanical systems such as a quadcopter with changing mass and rotational inertia is possible with the same mathematical framework. The typical model of such a system is given as

$$\begin{aligned}
\dot{\mathbf{x}}(t) &= \mathbf{A}(t)\mathbf{x}(t) + \mathbf{B}(t)\mathbf{u}(t) \\
\mathbf{y}(t) &= \mathbf{C}(t)\mathbf{x}(t) + \mathbf{D}(t)\mathbf{u}(t)
\end{aligned} \tag{9}$$

where, $\mathbf{x}(t)$ is the state vector, $\mathbf{u}(t)$ is the control input, $\mathbf{y}(t)$ is the output, and $\dot{\mathbf{x}}(t)$ is the rate of change of the system's state. The coefficients of these vectors are the state transition matrix $\mathbf{A}(t)$, the input matrix $\mathbf{B}(t)$, the output matrix $\mathbf{C}(t)$, and the feed-forward matrix $\mathbf{D}(t)$. In this study, state vector and control input vector of quadcopter defined as follows (10).

$$\mathbf{x} = \begin{bmatrix}\boldsymbol{\zeta} \\ \boldsymbol{\eta} \\ \mathbf{V} \\ \boldsymbol{\omega}\end{bmatrix} \in \mathbb{R}^{12} \quad , \quad \mathbf{u} = \begin{bmatrix}F_T \\ \mathbf{U}_T\end{bmatrix} \in \mathbb{R}^4 \tag{10}$$

In its most general form, rate of change of system state is given as

$$\dot{\mathbf{x}} = f(\mathbf{x}, \mathbf{u}) \tag{11}$$

Expanding (11) gives

$$\begin{bmatrix}\dot{x}_1 \\ \dot{x}_2 \\ \dot{x}_3 \\ \dot{x}_4 \\ \dot{x}_5 \\ \dot{x}_6 \\ \dot{x}_7 \\ \dot{x}_8 \\ \dot{x}_9 \\ \dot{x}_{10} \\ \dot{x}_{11} \\ \dot{x}_{12}\end{bmatrix} = \begin{bmatrix} x_7 \\ x_8 \\ x_9 \\ x_{10} + x_{12}c(x_4)t(x_5) + x_{11}s(x_4)t(x_5) \\ x_{11}c(x_4) - x_{12}s(x_4) \\ x_{12}c(x_4)sc(x_5) + x_{11}sc(x_5)s(x_4) \\ -\dfrac{F_T(c(x_4)c(x_6)s(x_5) + s(x_4)s(x_6))}{m} \\ \dfrac{F_T(c(x_6)s(x_4) - c(x_4)s(x_5)s(x_6))}{m} \\ g - \dfrac{F_T c(x_4)c(x_5)}{m} \\ \dfrac{U_2}{I_x} + \dfrac{(I_y - I_z)x_{11}x_{12}}{I_x} \\ \dfrac{U_3}{I_y} + \dfrac{(-I_x + I_z)x_{10}x_{12}}{I_y} \\ \dfrac{U_4}{I_z} + \dfrac{(I_x - I_y)x_{10}x_{11}}{I_z}\end{bmatrix} \tag{12}$$

As clearly seen above the trigonometric functions are one of the sources of non-linearity. We choose hover state as the point of linearization. The state and input at this equilibrium point are

$$\mathbf{x}_e = \begin{bmatrix}\boldsymbol{\zeta} \\ \mathbf{0}_{2\times1} \\ \psi \\ \mathbf{0}_{6\times1}\end{bmatrix}, \mathbf{u}_e = \begin{bmatrix}mg \\ \mathbf{0}_{3\times1}\end{bmatrix} \tag{13}$$

We use first-order Taylor series expansion to linearize around the equilibrium state to obtain

$$\mathbf{f}(\mathbf{x}, \mathbf{u}) = \begin{bmatrix}\mathbf{V} \\ \boldsymbol{\omega} \\ -g\theta \\ g\phi \\ -F_T/m \\ U_2/I_x \\ U_3/I_y \\ U_4/I_z\end{bmatrix} \tag{14}$$

Since the quadcopter system has 12 outputs, $\mathbf{C} = \mathbf{I}_{12x12}$ is identity matrix. In this study, the controller has no feed-forward block, so the feed-forward matrix $\mathbf{D}$ is equal to the zero matrix of size [12x4].

In this study, since the different payloads were mounted to quadcopter, inertia and moment of inertia are not constant. Matrix $\mathbf{B}$ contain m, I_x, I_y and I_z, since these values are variable, the system is a linear time varying system.

IV. Quadcopter Controller Design

A. Cascade Control

A system that has different response rates in its dynamic structure is difficult to control with a single control loop. Cascade controller can be used to control such complex systems. Cascade controller consists of two stages, the inner loop and the outer loop. In the cascade controller, the time constant of the inner loop must be less than the time constant

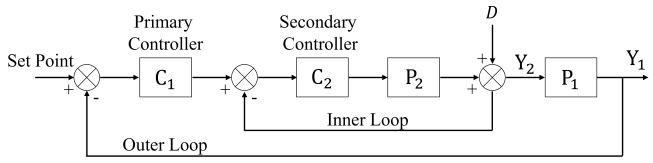

Fig. 2. Block diagram of cascade controller.

of the outer loop. The general structure of the cascade control system is shown in "Fig. 2".

Here P_1 and P_2 consist of the system's plant. The primary controller, C_1, sets the reference input of the inner loop. Hence C_1 regulates Y_1 which is primary controlled variable. The secondary controller, C_2, eliminates the disturbance effects before Y_2 signal it entries to P_1.

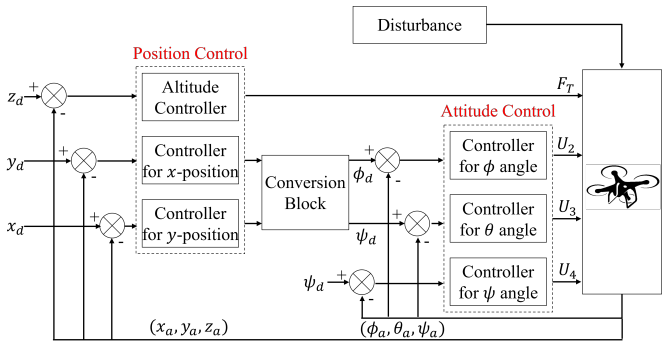

Fig. 3. The control system of the quadcopter.

The quadcopter control structure, consisting of the position controller and the attitude controller, is given in "Fig. 3". According to the linearized model of the system, the outputs to be controlled consist of x, y, z, and ψ, and the control inputs of the system are F_T, U_2, U_3, and U_4 respectively. All control blocks in "Fig. 2" are in a cascade structure. Since there are 2 PID controllers in each block, a total of 12 PID controllers, that is, 36 PID gain parameters, were used. The velocity expressions in (15) depend on the acceleration of gravity, not on the behavior of the four rotors. The outer control loop cannot be designed in this manner since the outcomes will be different on the real system.

$$\begin{aligned} \dot{u} &= -g\theta \\ \dot{v} &= g\phi \end{aligned} \tag{15}$$

The trigonometric relationship between angles and translational velocity is lost after linearization. Since the design is based on the control model, this non-linearity was applied to the controller with the inverse relationship in (16) and used in the conversion block.

$$\begin{aligned} \phi_d &= arcsin(\frac{u_y}{g}) \\ \theta_d &= -arcsin(\frac{u_x}{g}) \end{aligned} \tag{16}$$

In this paper, system controller coefficients were determined using the Ziegler Nichols method and PID tuner.

B. Gray Wolf Optimization Algorithm Based Cascade Control

The gray wolf optimization (GWO) algorithm, a nature-inspired optimization algorithm, is proposed by imitating the hunting behavior and social behavior of gray wolves. The social hierarchy of gray wolves are classified as alpha, beta, delta and omega. Candidate solutions are obtained by considering the social hierarchy of wolves. The solutions with the best fitness values are alpha, beta, delta and omega, respectively. The search for the best solution takes place in 3 stages: searching for prey, encircling prey, attacking prey. At the beginning of the optimization process, the gray wolf searches for its prey (possible solution) by randomly updating its position. In the encircling prey, gray wolves move in hyper-cubes (or hyper-spheres) around the best solution obtained. In the attacking section, alpha, beta and delta types of gray wolves have a well knowledge of the current location of the prey. Therefore, the first three best solutions obtained are saved and the positions of the other wolves are updated based on their best results. When the cost function converges to a given point, it approaches the optimal value. Gray wolves attack it to end the hunting. Pseudo code of the algorithm was given in "Fig. 4".

```
Initialize a population of gray wolves randomly
Evaluate fitness function to determine the fitness value of each wolf
Set alpha, beta, and delta as the three best wolves in the population
while termination criterion is not met do
    for each wolf i in the population do
        Calculate the distance between the current wolf i and alpha, beta, and delta
        Update the position of wolf i using the following formula:
        x_i = (α+2×β+2×δ−5×x_i)/4
        Apply a randomization operator to the new position of wolf i
        Evaluate the fitness value of the new position of wolf i
        if the new position is better than the position of alpha, beta, or delta then
            if the new position is better than alpha then
                Set the new position as alpha
            else if the new position is better than beta then
                Set the new position as beta
            else
                Set the new position as delta
            end if
        end if
    end for
end while
return alpha
```

Fig. 4. Pseudo code of gray wolf optimization [26].

As part of this study, integrated absolute error was used as the fitness function and is given in (17)

$$f_{IAE} = \int_0^t |e(t)|\, dt \tag{17}$$

here $e(t)$ represents the error and the aim of optimization is to minimize the error in the primary and secondary controller inputs that form the cascade controller. The optimization process was performed separately for x, y, z, and ψ, taking into account the computational load. In this work, the fitness functions of the controllable outputs of the system are given

as follows (18)

$$\begin{aligned} f_1 &= PID(e_x) + PID(e_u) + PID(e_\theta) + PID(e_q) \\ f_2 &= PID(e_y) + PID(e_v) + PID(e_\phi) + PID(e_p) \\ f_3 &= PID(e_z) + PID(e_w) \\ f_4 &= PID(e_\psi) + PID(e_w) \end{aligned} \tag{18}$$

where the expanded version of the $PID(e_x)$ controller is $u(t) = K_p e_x(t) + K_d \frac{\mathrm{d}}{\mathrm{d}t} e_x(t) + K_i \int_0^t e_x(\tau) d\tau$. The expression $e_x(t) = x_d(t) - x_a(t)$ indicates the error for the position x. Similar terms in the controller and error terms above can be expanded in the same way. In addition, the PID terms were not written in common brackets as they have different gain parameters. The purpose of the GWO in the study is to determine the gain parameters that minimize each fitness function. The block diagram of the optimized cascade controller that controls the quadcopter is shown in "Fig. 5".

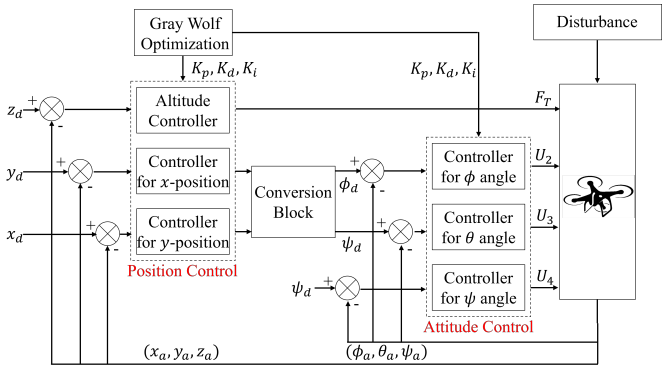

Fig. 5. Optimized cascade control system of the quadcopter.

In this study, different amounts of payloads are rigidly connected to the quadcopter. The gain parameters of the cascade controller used in the quadcopter control process, according to different payload, were obtained with the gray wolf optimization algorithm. Since it is not possible to change the gain parameters in the real-time application due to the long optimization time, the quadcopter system controller gain parameters was optimized according to the total mass values of 0.95, 1, 1.05 and 1.1. The optimized PID gain parameter sets are automatically selected based on the time-varying payload values supplied to the quadcopter. A linear interpolation based lookup table of the parameters was created according to the payload values used in the relevant ranges. Linear interpolation is given as follow (19)

$$a = a_1 + \frac{b - b_1}{b_2 - b_1}(a_2 - a_1) \tag{19}$$

where a, a_1, a_2, b, b_1, and b_2 points are shown in "Fig. 6".

To increase the performance of the controller, 36 PID parameters were optimized for specific payload values. As a result, optimized gain parameters were used according to the changing amount of payload.

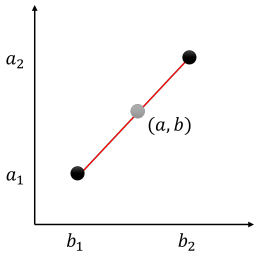

Fig. 6. Linear interpolation.

V. Simulation Results

A simulation study of the payload system rigidly connected on the quadcopter was carried out in two different trajectories. The first trajectory is in a helical shape as seen in "Fig. 7", and cascade and GWO-cascade controllers were applied to control the quadcopter system.

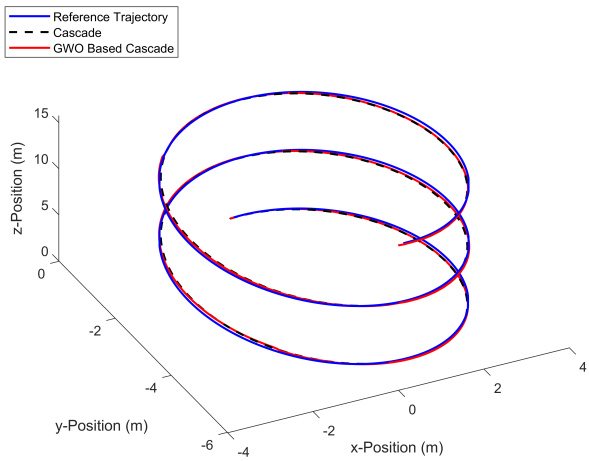

Fig. 7. Trajectories followed by the quadcopter payload system with different controllers applied.

The deviation of the quadcopter's position was calculated based on the distance between the reference point and the actual point and displayed in diagram "Fig. 8". Then, the total error amount was calculated according to IAE and it was found to be 20.9 m for the cascade controller and 2.474 m for the GWO-cascade controller. These results show that the performance of the controller was improved by about 88.1%.

Orientation errors occur while the quadcopter follows the trajectory. The difference between the reference orientation and the actual orientation results in the orientation error. In order to determine this difference, the reference Euler angles and the actual Euler angles were converted into axis angle representation. The amount of deviation in orientation was calculated by performing dot product between the reference and the actual vectors obtained from the axis angle in "Fig. 9". While the total error in the orientation according to IAE with the application of the cascade controller was 0.7805 rad, this result changed to 0.143 rad in the GWO-cascade controller.

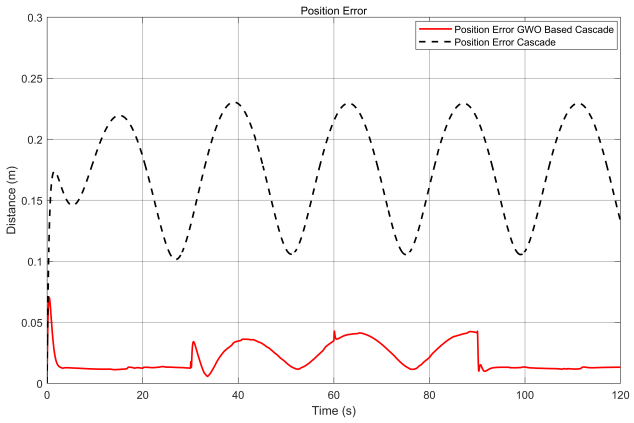

Fig. 8. Comparison of controller performances according to position error.

These results show that the performance of the controller could be improved by approx. 81.6%.

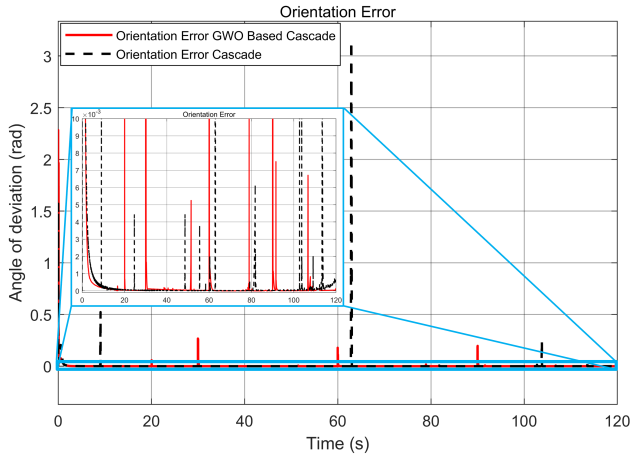

Fig. 9. Comparison of controller performances according to orientation error.

The second trajectory consists of continuous and discontinuous parts as seen in "Fig. 10", and cascade and GWO-cascade controllers were applied to control the quadcopter system. In this trajectory, abrupt changes in the roads lead to discontinuities in the trajectory.

The deviation of the quadcopter's position was calculated based on the distance between the reference point and the actual point and displayed in a diagram "Fig. 11". The total deviation of error was then calculated according to IAE and found to be 19.14 m for the cascade controller and 3.201 m for the GWO-cascade controller. These results show that the performance of the controller could be improved by approximately 83.3%.

Orientation errors occur while the quadcopter is following the flight path. The difference between the reference orientation and the actual orientation results in the orientation error. To determine this difference, the reference Euler angles and the actual Euler angles were converted into axis angle representation. The amount of deviation in orientation was

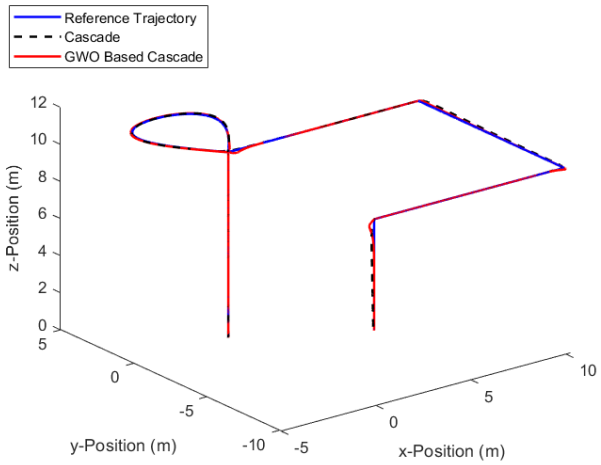

Fig. 10. Discontinuous trajectories followed by the quadcopter payload system with different controllers applied.

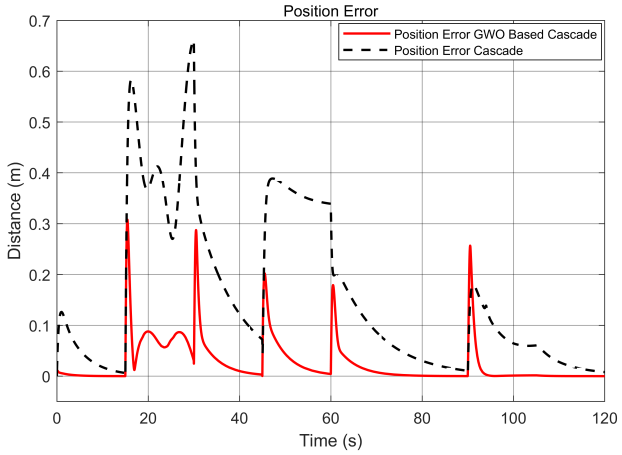

Fig. 11. Comparison of controller performances with respect to position error in discontinuous trajectory.

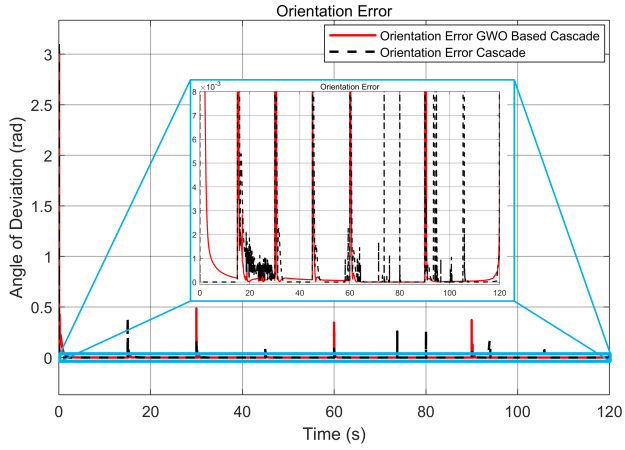

Fig. 12. Comparison of controller performances with respect to orientation error in discontinuous trajectory.

calculated by performing dot product between the reference and actual vectors obtained from the axis angle in "Fig. 12". While the total error in the orientation according to IAE was 0.1257 rad when using the cascade controller, this result changed to 0.2966 rad with the GWO cascade controller. These orientation results show that the performance of the cascade controller is better than that of the GWO-cascade in the second trajectory. However, while the GWO-cascade controller is better at resetting the error amount, as can be seen in "Fig. 12", the cascade controller made an oscillatory motion. The orientation error of the GWO-cascade controller is caused by peaks at the points where the PID parameters change.

VI. Conclusion

In this study, the transportation of a time-varying payload, which is rigidly connected to the quadcopter along the reference trajectory is discussed. The kinematic and dynamic analysis of the system was carried out and then the non-linear mathematical model was linearized using Taylor's series expansion. A linear time-varying state space model was created with the help of a linearized mathematical model. Since it is difficult to control a system with different response rates in its dynamic structure with a single control loop, a cascade controller was designed. The gain parameters were optimized with the GWO to increase the performance of the corresponding controller and maintain its stability against time-varying payloads. The optimization process was applied for 4 different payload values and the optimal gain parameters were determined within a certain search space for each different payload value. Subsequently, the obtained gain parameters were simulated on continuous and discontinuous trajectories to test the performance of the controller. The controller maintained its stability against changing load values and the performance of the classic cascade controller increased.

Further research is required to develop the mathematical model can be created by taking into account the disturbance inputs and uncertainties that affect the dynamics of the system for outdoor flights. Optimum gain parameters can be obtained and applied to the controller on-fly. The PID gain parameters obtained as a result of the GWO for different payload values did not exhibit uniform behavior. More research is required to develop a deeper understanding of the relationship between payload variation and behavior of the PID gain parameters.

References

[1] T. Nguyen et al., "MAVNet: An effective semantic segmentation micro-network for MAV-based tasks," IEEE Robot. Autom. Lett., vol. 4, no. 4, pp. 3908–3915, 2019.

[2] A. E. Jiménez-Cano, D. Sanalitro, M. Tognon, A. Franchi, and J. Cortés, "Precise Cable-Suspended Pick-and-Place with an Aerial Multi-robot System," J. Intell. Robot. Syst., vol. 105, no. 3, p. 68, Jul. 2022.

[3] X. Liang, H. Yu, Z. Zhang, H. Liu, Y. Fang, and J. Han, "Unmanned Aerial Transportation System With Flexible Connection Between the Quadrotor and the Payload: Modeling, Controller Design, and Experimental Validation," IEEE Trans. Ind. Electron., vol. 70, no. 2, pp. 1870–1882, Feb. 2023.

[4] C. Kim, H. Lee, M. Jeong, and H. Myung. A morphing quadrotor that can optimize morphology for transportation. In 2021 IEEE/RSJ International Conference on Intelligent Robots and Systems (IROS), pages 9683–9689, 2021.

[5] J. Fishman, S. Ubellacker, N. Hughes, and L. Carlone, "Dynamic Grasping with a Soft Drone: From Theory to Practice,IEEE International Conference on Intelligent Robots and Systems, 2021, pp. 4214–4221.

[6] X. Liang, Z. Zhang, H. Yu, Y. Wang, Y. Fang, and J. Han, "Antiswing Control for Aerial Transportation of the Suspended Cargo by Dual Quadrotor UAVs," IEEE/ASME Trans. Mechatronics, pp. 1–14, May 2022.

[7] A. Akhtar, S. Saleem, and J. Shan, "Path Following of a Quadrotor with a Cable-Suspended Payload," IEEE Trans. Ind. Electron., vol. 70, no. 2, pp. 1646–1654, Feb. 2023.

[8] N. Zhao, Y. Luo, H. Deng, Y. Shen, and H. Xu. The deformable quadrotor enabled and wasp-pedal-carrying inspired aerial gripper. In 2018 IEEE/RSJ International Conference on Intelligent Robots and Systems (IROS), pages 1–9, 2018.

[9] D. Sanalitro, H. J. Savino, M. Tognon, J. Cortés, and A. Franchi, "Full-Pose Manipulation Control of a Cable-Suspended Load with Multiple UAVs under Uncertainties," IEEE Robot. Autom. Lett., vol. 5, no. 2, pp. 2185–2191, Apr. 2020.

[10] A. Tagliabue, M. Kamel, R. Siegwart, and J. Nieto, "Robust collaborative object transportation using multiple MAVs," Int. J. Rob. Res., vol. 38, no. 9, pp. 1020–1044, Aug. 2019.

[11] X. Han, R. Miyazaki, T. Gao, K. Tomita, and A. Kamimura, "Controller Design and Disturbance Rejection of Multi-Quadcopters for Cable Suspended Payload Transportation Using Virtual Structure," IEEE Access, vol. 10, no. October, pp. 122197–122210, 2022.

[12] K. Mohammadi, S. Sirouspour, and A. Grivani, "Control of Multiple Quad-Copters with a Cable-Suspended Payload Subject to Disturbances," IEEE/ASME Trans. Mechatronics, vol. 25, no. 4, pp. 1709–1718, Aug. 2020.

[13] Y. S. Sarkisov, M. J. Kim, A. Coelho, D. Tsetserukou, C. Ott, and K. Kondak, Optimal Oscillation Damping Control of cable-Suspended Aerial Manipulator with a Single IMU Sensor; Optimal Oscillation Damping Control of cable-Suspended Aerial Manipulator with a Single IMU Sensor, 2020.

[14] C. Gabellieri, Y. S. Sarkisov, A. Coelho, L. Pallottino, K. Kondak, and M. J. Kim, "Compliance Control of a Cable-Suspended Aerial Manipulator using Hierarchical Control Framework, "IEEE/RSJ International Conference on Intelligent Robots and Systems (IROS), pages 7196–7202, 2020."

[15] R. Miyazaki, R. Jiang, H. Paul, Y. Huang, and K. Shimonomura, "Long-reach aerial manipulation employing wire-suspended hand with swing-suppression device," IEEE Robot. Autom. Lett., vol. 4, no. 3, pp. 3045–3052, Jul. 2019.

[16] G. Loianno et al., "Localization, Grasping, and Transportation of Magnetic Objects by a Team of MAVs in Challenging Desert-Like Environments," IEEE Robot. Autom. Lett., vol. 3, no. 3, pp. 1576–1583, Jul. 2018.

[17] C. Y. Son, H. Seo, T. Kim, and H. Jin Kim, "Model Predictive Control of a Multi-Rotor with a Suspended Load for Avoiding Obstacles," in Proceedings - IEEE International Conference on Robotics and Automation, Sep. 2018, pp. 5233–5238.

[18] H. Xie, X. Cai, and P. Chirarattananon, "Towards cooperative transport of a suspended payload via two aerial robots with inertial sensing," in IEEE International Conference on Intelligent Robots and Systems, Oct. 2020, pp. 1215–1221.

[19] G. Li, A. Tunchez, and G. Loianno, "PCMPC: Perception-Constrained Model Predictive Control for Quadrotors with Suspended Loads using a Single Camera and IMU," in 2021 IEEE International Conference on Robotics and Automation (ICRA), May 2021, vol. 2021-May, pp. 2012–2018.

[20] S. Tang, V. Wüest, and V. Kumar, "Aggressive Flight with Suspended Payloads Using Vision-Based Control," IEEE Robot. Autom. Lett., vol. 3, no. 2, pp. 1152–1159, Apr. 2018.

[21] X. Liang, Y. Fang, N. Sun, and H. Lin, "A novel energy-coupling-based hierarchical control approach for unmanned quadrotor transportation systems," IEEE/ASME Trans. Mechatronics, vol. 24, no. 1, pp. 248–259, Feb. 2019.

[22] S. Yang and B. Xian, "Energy-Based Nonlinear Adaptive Control Design for the Quadrotor UAV System with a Suspended Payload," IEEE Trans. Ind. Electron., vol. 67, no. 3, pp. 2054–2064, Mar. 2020.

[23] J. F. Slabber and H. W. Jordaan, “Vision-Based Control of an Unknown Suspended Payload with a Multirotor,” in IEEE International Conference on Intelligent Robots and Systems, 2021, pp. 4875–4880.
[24] J. Wehbeh, S. Rahman, and I. Sharf, “Distributed Model Predictive Control for UAVs Collaborative Payload Transport,” in IEEE International Conference on Intelligent Robots and Systems, Oct. 2020, pp. 11666–11672.
[25] D. Sanalitro, M. Tognon, A. E. J. Cano, J. Cortes, and A. Franchi, “Indirect Force Control of a Cable-Suspended Aerial Multi-Robot Manipulator,” IEEE Robot. Autom. Lett., vol. 7, no. 3, pp. 6726–6733, Jul. 2022.
[26] M. A. Afşar ve H. Arslan , ”Optimizing PID Gains of a Vehicle using the state-of-the-art Metaheuristic Methods”, Academic Platform Journal of Engineering and Smart Systems, c. 11, sayı. 3, ss. 107-117, Eyl. 2023.